Research Article | Vol. 25, No. 22 | 30 Oct 2017 | OPTICS EXPRESS 27405
Optics EXPRESS

Plasmonic Luneburg lens antenna synthesized by metasurfaces with hexagonal lattices

KUANG CHENG CHEN, JIUN WEN YANG, YUEH-CHIEH YANG, CHANG FU KHIN, AND M. NG MOU KEHN*

Department of Electrical Engineering, National Chiao Tung University, Taiwan
**malcolm.ng@ieee.org*

Abstract: The metasurface lens composing of 2D periodic metallic patches on a grounded dielectric slab possesses several advantages such as being light, low-profile, compact, and also cheap to manufacture. In this paper, a Luneburg lens synthesized by a metasurface and designated for use as a surface wave antenna is proposed. Two types of unit cell will be compared, one whose surface wave modal dispersion varies significantly with the grazing direction and another that does not. In the context of being applied as surface wave antennas, it will be shown that the Luneburg lens synthesized by the latter kind of unit cell provides improved performance as compared to the former. Several aperture sub-efficiencies of the metasurface-based Luneburg-lens antenna shall be used for the characterization of the radiation. A prototype of the designed lens antenna has also been manufactured. Measurement results agree well with theoretical predictions and the efficacy of this device over a fairly wide bandwidth has been experimentally demonstrated.

OCIS codes: (350.4010) Microwaves; (240.5420) Polaritons; (240.6690) Surface waves.

References and links

1. J. A. Dockrey, M. J. Lockyear, S. J. Berry, S. A. R. Horsley, J. R. Sambles, and A. P. Hibbins, "Thin metamaterial Luneburg lens for surface waves," Electromagnetic and Acoustic Materials Group, Department of Physics and Astronomy, University of Exeter, Stocker Road, Exeter EX4 4QL, United Kingdom, March 2013.
2. O. Quevedo-Teruel, M. Ebrahimpouri, and M. Kehn, "Ultra wide band metasurface lenses based on off-shifted opposite layers," IEEE Antennas Wirel. Propag. Lett. **11**, 1362–1365 (2012).
3. M. Casaletti, F. Caminita, and S. Maci, "A Luneburg lens designed by using a variable artificial surface," Proc. IEEE Antennas Propag. Society Int. Symp. (APS/URSI), Jul. 11–17, 2010, 1–4 (2010).
4. L. Xue and V. F. Fusco, "Printed holey plate Luneburg lens," Microw. Opt. Technol. Lett. **50**, 378–380 (2007).
5. L. Xue and V. F. Fusco, "24 GHz automotive radar planar Luneburg lens," IET Microw. Antennas Propag. **1**(3), 624–628 (2007).
6. S. Maci, G. Minatti, M. Casaletti, and M. Bosiljevac, "Metasurfing: addressing waves on impenetrable metasurfaces," IEEE Antennas Wirel. Propag. Lett. **10**, 1499–1502 (2011).
7. M. Bosiljevac, Z. Sipus, M. Casaletti, F. Caminita, and S. Maci, "Designing horn antennas based on variable metasurface concept," Proc. 6th Europ. Conf. Antennas Propag. (EuCAP) 2012, 1692–1695 (2012).
8. M. Casaletti, F. Caminita, S. Maci, M. Bosiljevac, and Z. Sipus, "New type of horn based on variable metasurface," Proc. IEEE Antennas Propag. Symp. **2011**, 1048–1050 (2011).
9. X. Xiong, Y. Liu, Z. Yao, L. Zhang, and W. Li, "Design of a metasurface Luneburg lens with flared structure," 2014 3rd Asia-Pacif. Conf. Antennas Propag. 375–378 (2014).
10. M. Bosiljevac, M. Casaletti, E. Caminita, Z. Sipus, and S. Maci, "Non-uniform metasurface Luneburg lens antenna design," IEEE Trans. Antenn. Propag. **60**(9), 4065–4073 (2012).
11. R. Quarfoth and D. Sievenpiper, "Broadband Unit-Cell Design for Highly Anisotropic Impedance Surfaces," IEEE Trans. Antenn. Propag. **62**, 4143–4152 (2014).
12. G. Goussetis, A. P. Feresidis and J. C. Vardaxoglou, "Tailoring the AMC and EBG Characteristics of Periodic Metallic Arrays Printed on Grounded Dielectric Substrate onwards," IEEE Trans. Antennas Propag. **54**(1), 54 (1), 82–89 (2006).
13. O. Quevedo-Teruel, R. C. Mitchell-Thomas, T. M. McManus, S. A. R. Horsley, and Y. Hao, "Conformal surface lenses from a bed of nails," The 8th European Conference on Antennas and Propagation (EuCAP 2014), The Hague, 2014, pp. 269–270.
14. O. Quevedo-Teruel, "Controlled radiation from dielectric slabs over spoof surface plasmon waveguides," Prog. Electromagnetics Res. **140**, 169–179 (2013).

#300675 https://doi.org/10.1364/OE.25.027405
Journal © 2017 Received 23 Jun 2017; revised 6 Oct 2017; accepted 16 Oct 2017; published 24 Oct 2017

Optics EXPRESS

15. X. Wan, Y. B. Li, B. G. Cai, and T. J. Cui, "Simultaneous controls of surface waves and propagating waves by metasurfaces," Appl. Phys. Lett. **105**, 121603 (2014).
16. M. Ebrahimpouri, E. Rajo-Iglesias, and O. Quevedo-Teruel, "Wideband glide-symmetric holey structures for gap-waveguide technology," 2017 11th European Conference on Antennas and Propagation (EUCAP), Paris, 2017, pp. 1658–1660.
17. R. K. Luneburg, *Mathematical Theory of Optics* (Brown University Press, 1944). pp. 189–213.
18. Per-Simon Kildal, "Characterization of Directive Antennas," *Foundation of Antenna Engineering* (Kildal Antenn AB 2015), pp. 21–74.
19. W. L. Stutzman, "Systems Communication for Antennas," in *Antenna Theory and Design* (John Wiley & Sons, Inc 2013), pp.100–127.
20. M. Ng, M. Kehn, and L. Shafai, "Characterization of dense focal plane array feeds for parabolic reflectors in achieving closely-overlapping or widely-separated multiple beams," Radio Sci. **44**(3), 1–25 (2009).
21. W. V. Cappellen, "Efficiency and sensitivity definitions for reflector antennas in radio astronomy," SKADS MCCT Workshop, 26~30, Nov 2007.
22. L. Zhao, X. Chen, and C. K. Ong, "Visual observation and quantitative measurement of the microwave absorbing effect at X band," Rev. Sci. Instrum. **79**(12), 124701 (2008).
23. R. C. Mitchell-Thomas, O. Quevedo-Teruel, J. R. Sambles, and A. P. Hibbins, "Omnidirectional surface wave cloak using an isotropic homogeneous dielectric coating," Sci. Rep. **6**, 30984 (2016).

1. Introduction

Over the recent years, considerable amount of research has been put into the study of metamaterial surfaces known also as metasurfaces, which are able to support surface plasmon polaritons (SPPs) [1], being essentially traditional surface waves that propagate along the planar interface between a metal and a dielectric. Metasurfaces have proven to be suitable for the syntheses of flat and compact 2D lenses. One common type is the Luneburg lens, the successful syntheses of which using metasurfaces have been reported in prior studies of [2–10].

The unit cells employed in the two dimensionally periodic arrays for the syntheses of metasurface lenses had virtually all been of the type that entails square periodicities, typically along x and y. Most works found in the literature on metasurface lenses had assumed the use of surface-wave propagation along just a solitary principal direction (x or y) in the generation of the dispersion diagram for subsequent relation with the refractive indices required for the syntheses of the plasmonic lenses. Although periodic arrays of circular or bean-shaped patches have been reported in studies of metamaterials, the square unit cells involved remain inherently anisotropic. However, the surface-wave bending at all locations on any type of plasmonic lens should strictly be under the conditions of different incidence angles as the rays move from a region of a certain refractive index to another of a different [2,11]. This suggests an apparent flaw in the synthesis by using only one fixed principal surface-wave propagation direction for all points on the lens. This possible loophole may nonetheless still not be an issue but only if the surface-wavenumber at any given frequency remains the same for various propagation directions, i.e. directional isotropy of the surface-wave modal wavenumber. However, investigations of surface modal dispersion curves of other periodic structures with square lattices for various azimuth angles have shown considerable anisotropy, such as printed patches or holey metallic structures [2]. The anisotropy also depends on the electrical dimensions of the unit cell. The smaller it is compared to the wavelength, the more isotropic will be the lattice. In the case that the employed unit cell is anisotropic, it will be required to correct for angular variations of the dispersion curves that might otherwise lead to inaccurate syntheses of the required lenses. In this paper, we propose the use of hexagonal unit cells that possess reduced anisotropy of the surface-wave phase constant with respect to the azimuth propagation directions. A Luneburg lens has been designed with this unit cell to demonstrate the enhanced immunity of this type of unit cell.

2. Directional anisotropy of surface wave dispersion of square unit cells

An infinite array of square metallic patches etched over a grounded dielectric substrate unit cells is first considered, as sketched in Fig. 1 [12]. The period of the likewise quadratic unit

Optics EXPRESS

cell is p = 2 mm and the thickness of the slab is h = 1.28 mm with a relative permittivity of 10.2. For three side lengths of the patch, namely a = 0.4, 1.0, and 1.3, the dispersion curves simulated by *CST Microwave Studio* are given in Fig. 1. At any frequency, the refractive index n is simply the ratio of the surface wavenumber k_s to the free space wavenumber k_0 [13–15], i.e.

$$n = k_s / k_0 . \tag{1}$$

Hence, the n required by the various regions of a plasmonic lens may be synthesized by tailoring the patch size.

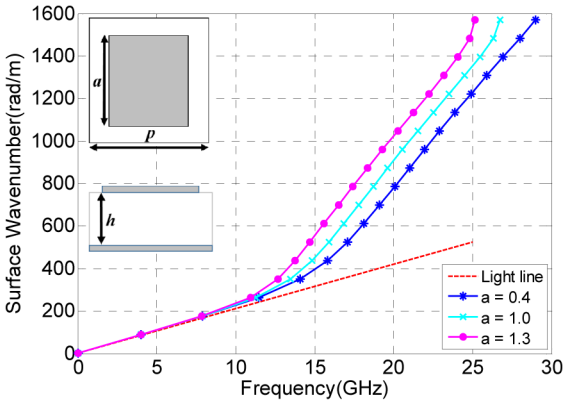

Fig. 1. Dispersion diagram of array of square patches printed on grounded substrate with square unit cell, for various patch sizes as annotated. p = 2 mm, h = 1.28mm.

Still on the preceding array of square patches within square unit cells, the dispersion for various azimuth angles of forcing grazing wavenumbers in the eigen-solver of the simulation software are presented in Fig. 2(a). Strong anisotropy at all frequencies is observed, evidenced by the fanned-out traces. This demonstrates the directional anisotropy of square (or rectangular in general) unit cells, thus leading to surface wavenumbers k_s that vary drastically with the azimuth direction of surface wave propagation. This would then result in synthesized n values that are likewise sensitive to this propagation direction. The fluctuation reaches as high as 13% as the surface-wave angles varies from 0 to 30 degrees at 12GHz. This calls for an alternative form of unit cell that provides alleviated sensitivity to the grazing angle.

3. Improved angular isotropy of hexagonal cells

For geometrical reasons, a square lattice can never be angularly isotropic in terms of azimuth directions of surface wave propagation. The most directionally insensitive shape that one could think of would be the circle, but then it is impossible to construct a continuously interconnected planar array of unit cells made out of such a shape. This then motivates or points to the next best but yet feasible shape, and that is the hexagon [16]. Intuitively, this is now a geometry that potentially offers reduced sensitivity to the azimuth angle.

Optics EXPRESS

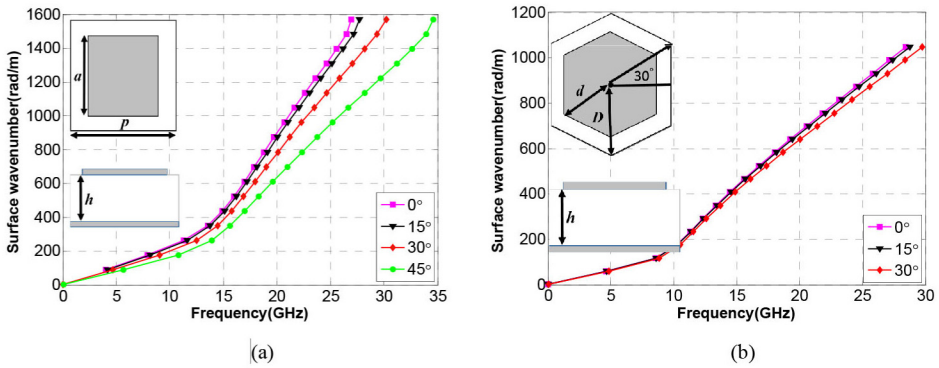

(a) (b)

Fig. 2. Dispersion for various azimuth angles as annotated, (a) square unit cell with p = 2 mm, h = 1.28 mm, and a = 1.8 mm, and (b) hexagonal unit cell with D = 2 mm, d = 0.9 mm, and h = 1.28 mm.

The dispersion diagram for the hexagonal unit cell is presented in Fig. 2(b), with the unit cell as shown inset, and for D = 2 mm, d = 0.9 mm, and h = 1.28 mm. It is easily observed that the surface wave number now has reduced variation with the azimuth angle as compared to the square lattice of Fig. 2(a). Indeed upon calculations, there is only about 5% variation between 0 and 30 degrees of incident angle at that same 12 GHz. The swept angle spans up to only 30 degrees (rather than 45) due to the irreducible Brillouin zone of the hexagonal cell.

4. Synthesis of a Luneburg lens

The Luneburg lens is a spherically symmetric gradient-index (GRIN) lens governed by the following relation [17]:

$$n = \sqrt{2 - (r/R)^2}. \tag{2}$$

where n is the refractive index, R is the radius of the lens and r denotes the radial location of any point in the lens. Hence, n is $\sqrt{2}$ at the center (r = 0) and unity at the outermost surface (r = R).

A Luneburg lens with radius R of 8 cm and composed of traditional square unit cells is first synthesized for operation at 12 GHz. The ideally continuous variation of n with the radial location within the lens is approximated in a stepwise fashion by subdividing the circular structure into ten concentric layers, the n in each being a discrete constant. A discrete port is used to excite a spherical wave from the edge of the structure. The simulated vertical z component of the electric field distribution is given in Fig. 3. As observed, despite the visible straightening of the curved wavefronts emanated by the discrete source upon arrival at the output aperture plane, the ray paths are somewhat still not quite ideally collimated enough, thereby compromising the quality of the aperture radiation.

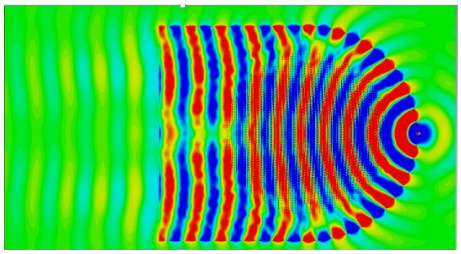

Fig. 3. E_z-field distribution of Luneburg lens composed of periodic square cells and excited by a point source at the right side of the lens at 12GHz.

Optics EXPRESS

In order to construct a new Luneburg lens, the aforementioned hexagonal unit cell has been employed. The radius is denoted as D and fixed to 1 mm, thereby with a resultant diameter of $2D = 2$ mm that equals the period p of the square lattice, whereas it is the radius d of the interior likewise hexagonal patch that is variable for adjustment to attain surface wavenumbers that can be translated to refractive indices. The dielectric constant of the substrate is chosen to be 10.2 and the height h is 1.28 mm. The required dimensions of the patches for achieving the Luneburg refractive indexes are represented in Fig. 4.

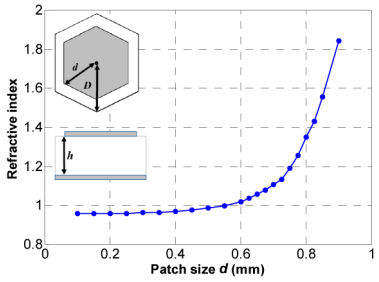

Fig. 4. Variation of refractive index with patch size or radius d of hexagonal patch within hexagonal unit cell.

Motivated by the investigations of Section III, the unit cells within the approximately half portion (semicircle) of the circular lens in which most of the ray-path bending occurs are replaced by hexagonal unit cells whereas the remaining semicircular region in which the surface-wave propagation directions are ideally parallel and straight shall be synthesized by unit cells that retain the square periodic arrangement, for the heightened ease and precision in the subsequent fabrication of a prototype of this design as well as for cost reduction. This is schematized in Fig. 5.

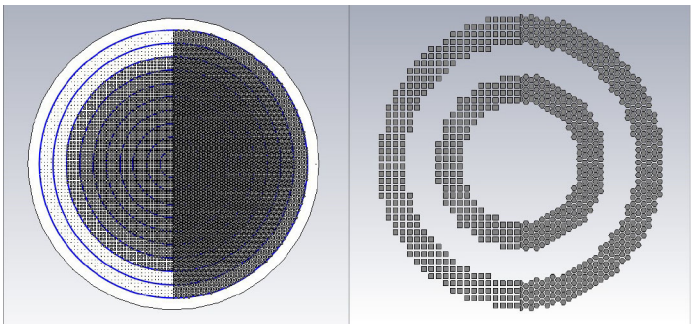

(a) (b)

Fig. 5. Luneburg lens composed of both hexagonal (in one semicircle) and square (the other half) lattice arrangements: (a) top view, and (b) zoomed-in illustration of the third and fifth layers.

The simulated E-field distribution of this Luneburg lens synthesized by a hybridized array of hexagonal and square unit cells is given in Fig. 6(a). As seen, the collimation of the rays is now considerably improved over that of Fig. 3 for the corresponding lens synthesized by purely square cells. Particularly, the wavefronts are now more well flattened out at the output aperture, attributed to the more properly bent surface-wave ray paths, especially in the immediate vicinity of the discrete source port. For plasmonic lens antennas synthesized by both the traditional way comprising purely square cells and the refined approach entailing hexagonal cells, the far field directive gain patterns in H-plane of both synthesis versions of the otherwise identical surface-wave antenna were also simulated and presented in Fig. 6(b).

An increase in the directivity from 12.4 dB for the lens antenna synthesized by square cells to 15.3 dB for the same configuration but composed of hexagonal lattice is observed.

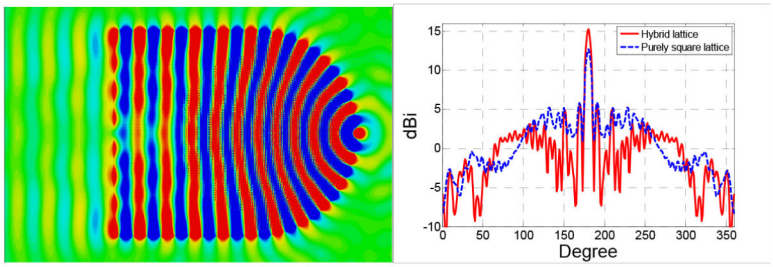

(a) (b)

Fig. 6. (a) E_z-field distribution of Luneburg lens synthesized by hybridized array of hexagonal and square unit cells, and (b) directivity patterns in H plane for Luneburg lens antenna synthesized by purely square lattices, and hybrid of square and hexagonal cells.

The radiation properties of such surface-wave antennas derived from the Luneburg lens may be quantified by the well-known subefficiencies that characterize radiating apertures. Under ideal lossless conditions, the antenna gain G can be expressed as [18,19]:

$$G = \varepsilon_{ap} D = \varepsilon_{ap} \frac{4\pi}{\lambda^2} A_p = \frac{4\pi}{\lambda^2} A_e. \tag{3}$$

where λ is the wavelength, D is the maximum available directivity stated as $4\pi/\lambda^2$ times the physical aperture area A_p, which in turn is diminished to an effective aperture A_e by a fraction defined as the aperture efficiency ε_{ap} that comprises the polarization, phase, and illumination subefficiencies. With $\vec{E}_{co}$ and $\vec{E}_{cross}$ denoting the co and cross polar E-field vector functions, respectively, these aperture sub efficiencies are mathematically expressed as follow [20, 21].

$$\varepsilon_{pol} = \frac{\int_A \left|\vec{E}_{co}\right|^2 ds}{\int_{A_p} \left(\left|\vec{E}_{co}\right|^2 + \left|\vec{E}_{cross}\right|^2\right) ds}. \tag{4}$$

$$\varepsilon_{ph} = \frac{\left|\int_{A_p} \vec{E}_{co} ds\right|^2}{\left(\int_{A_p} \left|\vec{E}_{co}\right| ds\right)^2}. \tag{5}$$

$$\varepsilon_{ill} = \frac{1}{A} \frac{\left|\int_{A_p} \vec{E}_{co} ds\right|^2}{\int_{A_p} \left|\vec{E}_{co}\right|^2 ds}. \tag{6}$$

The flat and open nature of such surface-wave antennas based on the Luneburg lens is beneficial to the savings of space and weight. While the diameter of the circular 2D structure may rationally dictate the span of one dimension of A_p (particularly, the horizontal one), the absence of a third (vertical) dimension of the output radiating port means that a well-defined physical aperture cannot be perceived as readily as conventional antennas such as horns, reflectors, and arrays. In order to calculate the efficiencies, the simulated field data of each point on the aperture was processed and applied to the expressions in (4) to (6) for the various subefficiencies. Comparisons of these figures-of-merit between the Luneburg lens antenna

Optics EXPRESS

synthesized entirely by traditional square lattices and its counterpart comprising a combination of hexagonal and square unit cells (one semicircle each) are presented in Fig. 7. As observed, all three performance indices of the hybridized version are enhanced beyond those of the case composed of purely square cells.

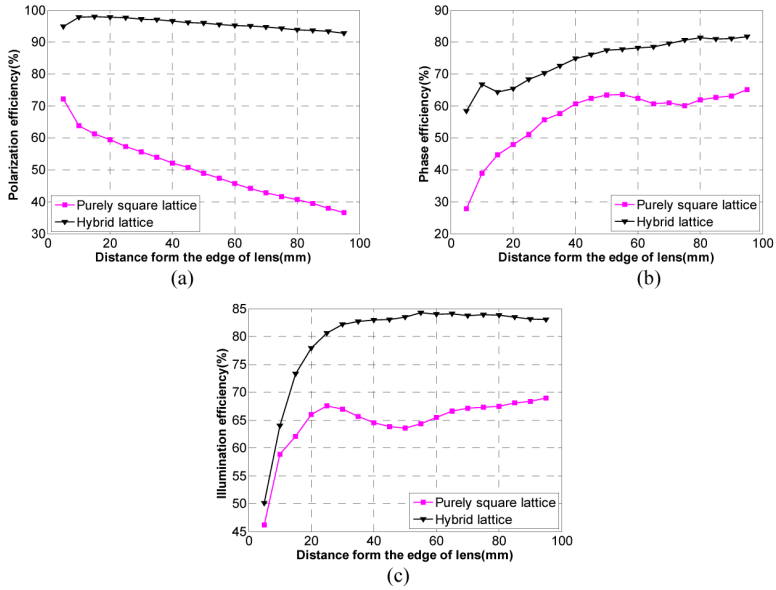

Fig. 7. Comparison of subefficiencies between Luneburg lens antenna synthesized by traditional "entirely square cells" way and new approach composed of square and hexagonal cells; (a) polarization efficiency (b) phase efficiency, and (c) illumination efficiency.

5. Experimental results of fabricated prototype

A prototype of the Luneburg lens with that same R = 8 cm and composed of square and hexagonal lattices has been manufactured, a photograph of which is given in Fig. 8(a). Placed alongside in Fig. 8(b) is the schematic of the experimental setup for measuring the focusing effects of the lens [22].

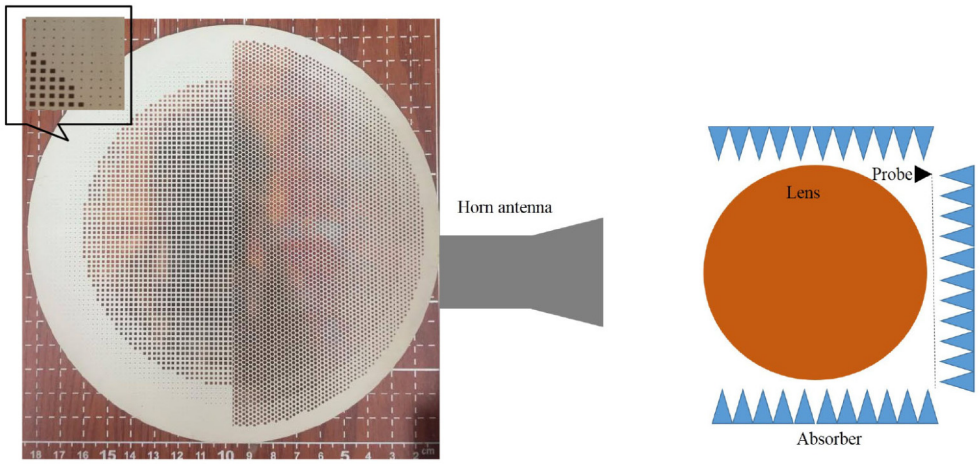

Fig. 8. (a) Photograph of a fabricated Luneburg lens synthesized by hexagonal and square unit cells (one semicircle for each), and (b) experimental setup

Optics EXPRESS

A two-port vector network analyzer was used for the measurements. Connected to one port, a Ku-band horn antenna was used to illuminate the lens placed in its far field with a planar wavefront. An SMA probe with protruded inner rod length of 6 mm and connected to the other port was then swept throughout the surface of the lens and the measured S-parameters were consequently translated to relay the field pattern [23], as presented in Fig. 9(a), as well as the phase pattern of the wavefront in Fig. 9(b), for the design frequency of 12 GHz. The convergence of the wavefront towards a focal point with maximum field intensity is clearly visible. The focusing is further conveyed by the three subplots of Fig. 10, each presenting the graph of the measured field versus the dimension along the breadth of the planar aperture containing the focal point at one of three frequencies as labeled. Clearly, the peaking of the field strength at the focal point is observed at all frequencies, with the best performance showing up at the designated 12 GHz.

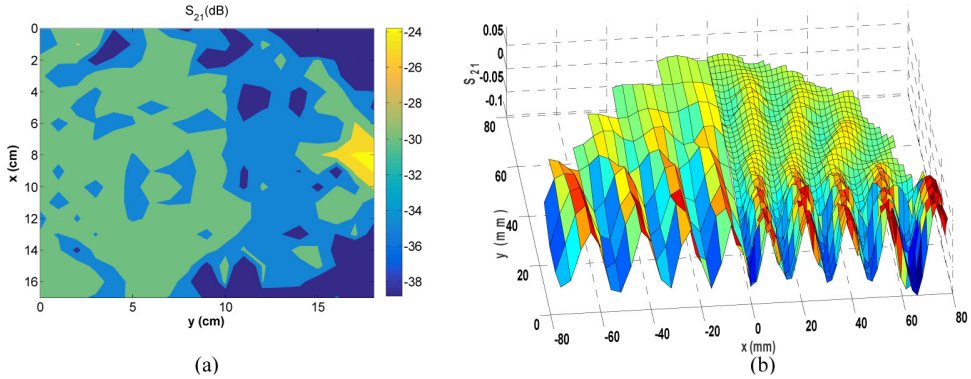

Fig. 9. Measured (a) amplitude distribution, and (b) phase pattern of wavefront over surface of lens at 12 GHz. Because of symmetry, only one half is required for the phase pattern. Due to the time-consuming and labor-intensive nature of the measurements, resolution of measured data points made high only in upper right quadrant of wavefront pattern in which bending towards the focal point at (x = 0, y = 80) occurs. Upper left quadrant containing essential planar wavefronts clearly visible despite coarser resolution.

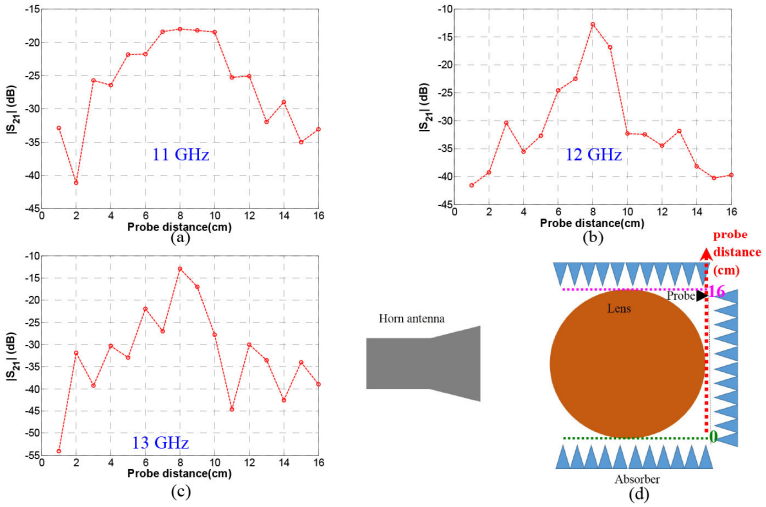

Fig. 10. Graphs of measured field level plotted versus the dimension along the breadth of the planar aperture containing the focal point; for (a) 11 GHz, (b) 12 GHz, (c) 13 GHz, and (d) illustration of axis for probe distance in graphs (a) to (c), with indicated locations of 0 and 16 cm.

Optics EXPRESS

The far-field radiation patterns of the manufactured Luneburg lens antenna were also measured in an anechoic chamber, as presented in Fig. 11 and in which simulated patterns are included. Good agreement in terms of the directivity and width of the main beam between experiment and simulation is observed. Discrepancies in the levels of the sidelobes could be attributed to the very fact that the excitation feeds for both scenarios are fundamentally different; being just an idealized discrete source (placed at the focal point) in the simulation software environment which is indeed more omnidirectional (explaining the higher sidelobes), whereas a small waveguide opening was instead adopted as the input port for the measurements (also mounted at the focus, of course). Besides, the sidelobe levels of the measurements are even lower than those from simulations, which in fact is a favored outcome.

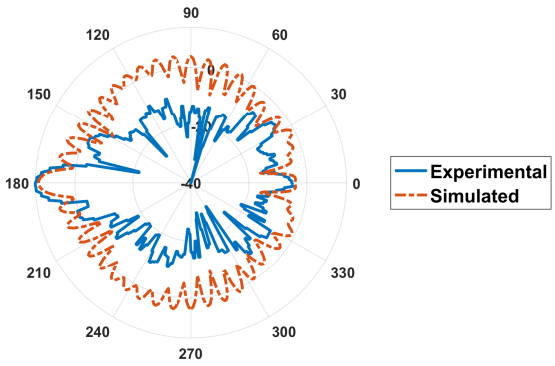

Fig. 11. Measured far-field radiation patterns of manufactured Luneburg lens antenna, with simulated patterns included. Good agreement of maximum directive gain level and width of main beam between simulation and experiment observed.

6. Conclusions

This paper has addressed the apparent flaw with the traditional use of just a principal direction of anisotropic square periodic arrays in the generation of surface-wave modal dispersion attributes for subsequent use in synthesizing the various refractive indices required by any metasurface lens. A novel unit cell has been proposed, one that is hexagonally shaped and which encases a likewise hexagonal patch, being a geometry that is intuitively more isotropic. The array composed of it has indeed been demonstrated to be less sensitive to the surface-wave propagation direction. Using the Luneburg lens as a vehicle of the study, simulated field patterns of the lens synthesized by the mixed use of hexagonal and square lattices (the former for the semicircle in which the surface rays undergo the most curving towards the focal point) are indeed found to be superior to those of the counterpart structure composed purely of square unit cells. Besides just visual portrayal via field patterns, the improvement is further exemplified through the simulated radiation patterns of both contending versions, from which the directivity of the traditional one comprising entirely square cells being considerably lower than that of the proposed design entailing a hexagonal lattice. To still go one more step further, the usual aperture subefficiencies that quantify how well an antenna radiates have also been calculated and the enhanced levels of all figures-of-merit (polarization, phase, and illumination subefficiences) of the Luneburg-type plasmonic antenna made of both hexagonal and square cells as compared to those of its purely square-celled counterpart are again verified. Finally, a prototype of the refined lens design has been manufactured. Measured field distributions and phase patterns across the surface indeed display increased intensities that are concentrated within the region containing the plasmonic

Optics EXPRESS

wavefronts as expected from theory and the convergence of ray trajectories towards the focal point is also clearly demonstrated. This focusing ability is also found to be maintained over a fairly wide bandwidth about the design frequency at which the field localization at the focal point is at its strongest. Far-field radiation patterns of the manufactured Luneburg lens operated as an aperture antenna (with a source located at the focus) were also measured in an anechoic chamber, the results of which are in good agreement with simulations in terms of the directivity and beamwidth.

Funding

Ministry of Science and Technology of Taiwan (MOST 106-2221-E-009-021).

Acknowledgments

The authors are grateful to the Ministry of Science and Technology of Taiwan for supporting this work, and to Prof. Oscar Quevedo-Teruel for offering constructive comments and helpful suggestions. They are also thankful to Prof. T. C. Chiu of the National Central University (NCU), Taiwan, for providing the use of the anechoic chamber at NCU required for the measurements of the far-field radiation patterns.